BIOCHEMISTRY
including biophysical chemistry & molecular biology

Article

pubs.acs.org/biochemistry

Internal Motions and Exchange Processes in Human Ileal Bile Acid Binding Protein As Studied by Backbone ^{15}N Nuclear Magnetic Resonance Spectroscopy

Gergő Horváth, Péter Király, Gábor Tárkányi, and Orsolya Toke*

Institute of Structural Chemistry, Chemical Research Center of the Hungarian Academy of Sciences, 59-67 Pusztaszeri út, Budapest, H-1025 Hungary

Supporting Information

ABSTRACT: Human ileal bile acid binding protein (I-BABP), a member of the family of intracellular lipid binding proteins, is thought to play a role in the enterohepatic circulation of bile salts. Previously, we have shown by stopped-flow fluorescence analysis that positive binding cooperativity exhibited by I-BABP in its interactions with glycocholate (GCA) and glycochenodeoxycholate (GCDA), the two primary bile salts in humans, is related to a slow conformational change in the protein. In this study, we used backbone ^{15}N relaxation nuclear magnetic resonance (NMR) techniques to obtain residue-specific information about the internal dynamics of apo I-BABP and the doubly ligated I-BABP:GCA:GCDA complex on various time scales. According to our NMR data, bile salt binding is accompanied by a slight rigidification of the ^{15}N−^{1}H bond vectors on the picosecond to nanosecond time scale, with most pronounced changes occurring in the C−D region. In contrast to the minor effects of ligation on fast motions, relaxation dispersion NMR experiments indicate a marked difference between the two protein states on the microsecond to millisecond time scale. In the apo form, an extensive network of conformational fluctuations is detected throughout segments of the EFGHIJ β-strands and the C−D loop, which cease upon complexation. Our NMR data are in agreement with a conformational selection model we proposed earlier for I-BABP and support the hypothesis of an allosteric mechanism of ligand binding. According to the NMR measurements, the helical cap region may have a less crucial role in mediating ligand entry and release than what has been indicated for fatty acid binding proteins.

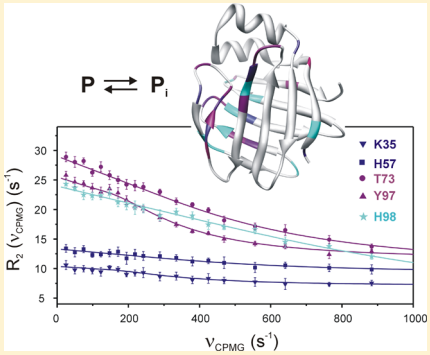

Bile salts are amphipathic molecules synthesized from cholesterol in the liver, which in the small intestine facilitate the absorption of dietary lipids, cholesterol, and fat-soluble vitamins.[1] Besides their role in digestion, they are also known as signal molecules that play a role in triglyceride, cholesterol, energy, and glucose homeostasis.[2,3] When a meal is ingested, bile salts are secreted into the proximal small intestine via the gall bladder and are efficiently recycled via a process termed enterohepatic circulation.[4] Human ileal bile acid binding protein (I-BABP), a member of the family of intracellular lipid binding proteins,[5,6] is thought to play a key role in this recycling process via binding interactions occurring within the absorptive epithelial cells of the ileum.

Previously, it has been shown that human I-BABP binds two molecules of glycocholate (GCA), the physiologically most abundant bile salt, with low intrinsic affinity but a high degree of positive cooperativity.[7] Calorimetric analysis of bile acid derivatives has indicated that positive cooperativity in bile salt−I-BABP recognition is governed by the pattern of steroid ring hydroxylation, rather than the presence and type of side chain conjugation.[8] In addition to binding cooperativity, I-BABP has been found to show a high degree of site selectivity in its interactions with GCA and glycochenodeoxycholate (GCDA) (Figure 1), the two primary bile salts in humans.[9] As a result,

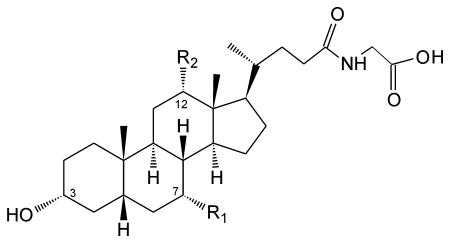

Figure 1. Chemical structure of glycocholic acid (GCA; R_1 = OH, and R_2 = OH) and glycochenodeoxycholic acid (GCDA; R_1 = OH, and R_2 = H).

while in homotypic complexes both bile salts occupy both sites, in the heterotypic I-BABP:GCDA:GCA complex (1.0:1.5:1.5), GCDA and GCA displace each other and selectively occupy sites 1 and 2, respectively. According to our previous mutagenesis study, cooperativity and site selectivity are not linked in the protein.[10] While cooperativity is governed by a subtle interplay of entropic and enthalpic contributions, site

Received: October 16, 2011
Revised: February 13, 2012
Published: February 13, 2012

selectivity is determined by more localized, enthalpic effects. On the basis of nuclear magnetic resonance (NMR) structural work and the mutagenesis study, two hydrogen bonding networks have been postulated as a likely way of energetic communication between the two binding sites.[10] It has also been shown by stopped-flow fluorescence analysis that a slow conformational change occurring after the second binding step has a role in positive cooperativity.[11] Furthermore, the unexpectedly slow association rate constant ($\sim$1 μM^{-1} s^{-1}) of the first binding step has raised the possibility of an additional conformational transition in the apo protein prior to binding. A conformational change on a similar time scale in the unbound state has been proposed previously for intestinal fatty acid binding protein (I-FABP),[12,13] and more recently for cellular retinol binding proteins (CRBP I and II)[14] and chicken liver bile acid binding protein (cl-BABP),[15] three other members of the iLBP family with the same topology. In all cases, the observed slow motion is thought to be associated with ligand entry and release.

As a first step in untangling the various dynamic events in I-BABP occurring on different time scales and elucidating their specific role in the binding process, we report here the chemical shift-based structure analysis and backbone ^{15}N relaxation NMR study of apo I-BABP and that of the heterotypic I-BABP:GCA:GCDA (1.0:1.5:1.5) complex.

MATERIALS AND METHODS

Protein Biosynthesis and Purification. The expression of uniformly ^{15}N-enriched and ^{13}C- and ^{15}N-enriched protein followed a two-stage strategy designed to achieve an optimal balance between cell growth and isotope utilization. Specifically, *Escherichia coli* strain MG1655, transformed with the pMON5840-hIBABP construct, was incubated overnight (37 °C and 250 rpm) in 50 mL of non-isotope-enriched minimal medium (6 g/L Na_2HPO_4, 3 g/L KH_2PO_4, 0.5 g/L NaCl, 1 g/L NH_4Cl, 1 mM $MgSO_4$, 5 g/L D-glucose, 25 mg/L thiamine hydrochloride, 0.1 mM $CaCl_2$, and trace metals, according to Li et al.[16]) containing 100 μg/mL ampicillin and then transferred into a 2 L flask containing 700 mL of medium of the same composition. At an OD_{600} of $\sim$1.0, the culture was centrifuged at 4 °C and 10000*g* for 15 min and the pellet was resuspended in 700 mL of fresh isotope-enriched minimal medium containing 0.7 g of $^{15}NH_4Cl$ (^{15}N-enriched and ^{13}C- and ^{15}N-enriched I-BABP) and 3.5 g of [^{13}C]-D-glucose (^{13}C- and ^{15}N-enriched I-BABP). Protein expression, under the control of the recA promoter, was induced by the addition of 7 mL of 10 mg/mL nalidixic acid to the growing culture at an OD_{600} of $\sim$2.0, and cells were allowed to grow for an additional 3−4 h, harvested, and frozen at −80 °C. For the uniformly (80% ^2H, 99% ^{15}N) enriched human I-BABP, a one-stage protocol was applied. Specifically, cells were grown in 800 mL of minimal medium in 99% D_2O supplemented with $^{15}NH_4Cl$ and natural abundance glucose at 37 °C for 19 h, induced at an OD_{600} of $\sim$2.4, and grown for an additional 4 h before being harvested. Protein purification started with thawing the cell pellet in 10 mL of 20 mM Tris-HCl (pH 8.0) and 5 mM EDTA, containing a broad-spectrum protease inhibitor mixture (Roche Molecular Biochemicals). The protein was released by processing the cell suspension through an Emulsiflex C5 homogenizor (Avestin) three or four subsequent times. The homogenized cell suspension was subjected to centrifugation at 4 °C and 23000*g* for 30 min. The clarified supernatant was chromatographed on a 25 cm × 5 cm column of Q-Sepharose Fast Flow. Dialysis was conducted versus multiple changes of 10 mM Tris (pH 8.2) and 0.05% NaN_3 at 4 °C, until the A_{260}/A_{280} absorbance ratio decreased below 0.7 followed by gel filtration chromatography using a 110 cm × 2.5 cm column of Sephadex G-50. Delipidation was achieved by passing the protein solution over a column of lipophilic Sephadex type VI (Sigma product no. H-6258) pre-equilibrated with 20 mM potassium phosphate, 50 mM KCl, and 0.05% NaN_3 (pH 6.3), at 37 °C. Protein purity, as assessed by overloaded Coomassie-stained sodium dodecyl sulfate−polyacrylamide gel electrophoresis gels, was >98%. Protein concentrations were determined by absorbance at 280 nm using an extinction coefficient of 12930 M^{-1} cm^{-1} obtained by composition analysis according to Pace et al.[17]

Collection of NMR Data. Multidimensional NMR experiments were conducted at 25 °C on 600 and 400 MHz *Varian NMR SYSTEM* spectrometers equipped with a 5 mm indirect detection triple $^1H^{13}C^{15}N$ and double resonance ^1H-{^{15}N-^{31}P} *z*-axis gradient probe, respectively. Measurements were taken in a buffer containing 20 mM potassium phosphate, 50 mM KCl, and 0.05% NaN_3 (pH 6.3). The protein concentration was 1 mM in all experiments. In the case of the holo sample, protein was complexed with an equimolar mixture of GCA and GCDA at an I-BABP:GCA:GCDA molar ratio of 1.0:1.5:1.5, ensuring that more than 99.9% of the protein was in its bound state.[8]

The backbone resonance assignment strategy utilized uniformly ^{13}C- and ^{15}N-enriched wild-type human I-BABP and a series of three-dimensional (3D) gradient-enhanced triple-resonance experiments such as g-HNCACB,[18−20] g-CBCA-CONNH,[21] g-HNCO,[19,20,22,23] and g-HCACON.[24] Spectral processing, computer-assisted spin system analysis, and resonance assignment were conducted with Felix 2004 (Accelrys, Inc.). The ^1H chemical shift was referenced externally to 2,2-dimethylsilapentane-5-sulfonic acid (DSS), and the ^{13}C and ^{15}N chemical shifts were referenced indirectly to DSS.[25] Chemical shift indices were calculated from the $^1H_\alpha$, $^{13}C_\alpha$, $^{13}C_\beta$, and ^{13}CO chemical shifts using CSI.[26]

The ^{15}N T_1, T_2, and steady-state {^1H}−^{15}N NOE measurements[27−29] were collected on uniformly ^{15}N-enriched apo and holo human I-BABP at two static magnetic field strengths, 14.1 and 9.4 T (corresponding to ^1H Larmor frequencies of 600 and 400 MHz, respectively). Backbone amide ^{15}N T_1 values were measured from two series of eight spectra (24 transients, interscan delay of 1.5 s) with the following relaxation delay times: 20, 100, 190, 290, 390, 530, 670, and 830 ms and 20, 50, 100, 170, 240, 340, 480, and 630 ms. Amide ^{15}N T_2 values were obtained similarly: 10, 30, 50, 70, 110, 150, and 190 ms and 10, 30, 50, 90, 130, 150, and 170 ms. Steady-state {^1H}−^{15}N NOE values were obtained by recording spectra with and without (blank) the use of ^1H saturation applied during the last 5 s of a 7 s delay between successive transients. Presaturation was achieved with the use of 120° ^1H pulses applied every 5 ms.[30] The radiofrequency field strength of the ^1H hard pulse was 11.6 kHz. To map regions of backbone order and disorder, gradient- and sensitivity-enhanced ^{15}N HSQC experiments were used to collect amide proton saturation transfer data by recording spectra with and without water presaturation during a 3 s interscan delay. NOE and saturation transfer measurements (32 transients both) were collected in triplicate.

Relaxation dispersion experiments were performed at a static magnetic field strength corresponding to a proton Larmor frequency of 600 MHz, using a relaxation-compensated CPMG dispersion experiment performed in a constant time manner.[31,32] To reduce the R_2 of the H_zN_x coherence evolving

dx.doi.org/10.1021/bi201588q | *Biochemistry* 2012, 51, 1848−1861

during the CPMG periods, measurements were taken on uniformly 80% 2H- and 99% ^{15}N-labeled protein. The constant time delay (T_{CP}) was set to 40 ms. Spectra were collected as a series of 20 two-dimensional data sets with CPMG field strengths (ν_{CPMG}) of 25, 50, 74, 99, 123, 147, 172, 195, 219, 242, 289, 335, 380, 425, 469, 556, 641, 764, and 883 Hz. A reference spectrum was obtained by omitting the CPMG period from the pulse sequence.[33] Spectra (3 s interscan delay, 24 transients) were acquired in duplicate.

Relaxation and Model-Free Parameter Calculations. Initial processing of the relaxation, NOE, and saturation transfer measurements was conducted using the Biopack module of VNMRJ 2.2.C. For spectral analysis, the Fourier-transformed and phased spectra were imported into SPARKY.[34] Peak intensities were estimated from their peak heights. For both the T_1 and T_2 spectra, relaxation times were determined by fitting to a two-parameter function of the form

$$I(t) = I_o \exp(-t/T_{1,2}) \tag{1}$$

using the Levenberg−Marquardt[35] algorithm, where $I(t)$ is the peak intensity after a delay time of t and I_o is the initial intensity. For subsequent analysis, the standard errors of the T_1 and T_2 relaxation times were estimated from duplicate measurements at various relaxation delays. The NOE and amide hydrogen exchange values were calculated as a ratio of signal intensities with and without presaturation, and the uncertainty was estimated by repeating the experiments three times.

An initial estimate of the rotational diffusion anisotropy was calculated from the filtered T_1/T_2 ratios using the program r2r1_diffusion (http://www.palmer.hs.columbia.edu/software/r2r1_diffusion.html). The overall rotational correlation time (τ_m) calculated from the trace of the diffusion tensor was in a good agreement with the value obtained from a trimmed mean value of T_1/T_2 according to Kay et al.[36] For the accurate determination of rotational anisotropy, Protein Data Bank (PDB) entry 1O1U[37] was used for the apo protein. In the case of the holo form, both PDB entry 1O1V (a 1:1 complex of human I-BABP with taurocholate)[37] and the three-dimensional structure of the heterotypic doubly ligated complex (I-BABP:GCA:GCDA, 1.0:1.5:1.5) developed by Cistola and coworkers (ref 10 and personal communication with G. T. DeKoster, G. P. Tochtrop, J. D. Monsey, and D. P. Cistola) have been considered. The actual values of motional parameters presented are obtained using the coordinates of the latter. For comparison, the results of the analysis conducted with coordinates of 1O1V are included in Figures S3 and S4 of the Supporting Information. We note that no significant differences have been found in the distribution and amplitude of fast (picoseconds to nanoseconds) and slow (microseconds to milliseconds) fluctuations when using the two different sets of coordinates. The principal moments of inertia tensors for the models were calculated using the program PDBinertia (http://biochemistry.hs.columbia.edu/labs/palmer/software/pdbinertia.html).

Spectral densities were calculated from the ^{15}N relaxation parameters according to Abragam.[38]

$$T_1^{-1} = \frac{d^2}{4}[J(\omega_H - \omega_N) + 3J(\omega_N) + 6J(\omega_H + \omega_N)] + c^2 J(\omega_N) \tag{2a}$$

$$T_2^{-1} = \frac{d^2}{8}[4J(0) + J(\omega_H - \omega_N) + 3J(\omega_N) + 6J(\omega_H) + 6J(\omega_H + \omega_N)] + \frac{c^2}{6}[4J(0) + 3J(\omega_N)] + R_{ex,app} \tag{2b}$$

$$NOE = \frac{d^2}{4}[6J(\omega_H + \omega_N) - J(\omega_H - \omega_N)]\left(\frac{\gamma_H T_1}{\gamma_N}\right) + 1 \tag{2c}$$

The constants d^2 and c^2 are defined as $d = (\mu_o H_o \gamma_H \gamma_N / 8\pi^2)\langle r_{NH}^{-3}\rangle$ and $c = \omega_N \Delta\sigma/\sqrt{3}$, where γ_H and γ_N are the gyromagnetic ratios of the ^{1}H and ^{15}N nuclei, respectively, ω_H and ω_N are their Larmor precessional frequencies, respectively, r_{NH} is their internuclear distance (1.02 Å), $\Delta\sigma$ is the difference between the parallel and perpendicular components of an axially symmetric ^{15}N chemical shift tensor (−172 ppm for protein backbone amides[39]), and H_o is the external magnetic field strength. To obtain details of the amplitude and time scale of dynamic events, we analyzed the NMR relaxation data within the model-free formalism.[40−43] Information about the spatial restriction of the ^{15}N−^{1}H bond vector (S^2, generalized order parameter), the correlation time for macromolecular tumbling (τ_m) and that for internal motion (τ_e), and the contributions of microsecond to millisecond exchange phenomena to transverse relaxation ($R_{ex,app}$) have been determined using FAST-Modelfree (Facile Analysis and Statistical Testing for Modelfree[44]), an automated version of Modelfree 4.2,[45,46] a program used extensively to fit the extended model-free spectral density function

$$J(\omega) = \frac{2}{5}\sum_{j=1}^{3} A_j\left[\frac{S^2\tau_j}{1 + (\omega\tau_j)^2} + \frac{(1 - {S_f}^2)^2\tau_f'}{1 + (\omega\tau_f')^2} + \frac{({S_f}^2 - S^2)\tau_s'}{1 + (\omega\tau_s')^2}\right] \tag{3}$$

to NMR spin relaxation data, assuming an axially symmetric diffusion tensor, where ${\tau_1}^{-1} = 6D_\perp$, ${\tau_2}^{-1} = D_\parallel + 5D_\perp$, ${\tau_3}^{-1} = 4D_\parallel + 2D_\perp$, $\tau_s' = \tau_j\tau_e/(\tau_j + \tau_e)$, where τ_e is either τ_f or τ_s, $A_1 = (3\cos^2\theta - 1)^2/4$, $A_2 = 3\sin^2\theta\cos^2\theta$, $A_3 = {}^3/_4\sin^4\theta$, and θ is the angle between the N−H bond vector and the unique axis of the diffusion tensor. Briefly, five representations of the spectral density function were considered. The first model (M1) was based simply on the single-time scale model-free formalism given in eq 3 with fitting S^2 alone ($\tau_f = \tau_s = 0$). The next model (M2) incorporated the presence of fast internal motions ($\tau_f <$ 100−200 ps) by fitting both S^2 and $\tau_e = \tau_f$. The third (M3) and fourth (M4) models added an $R_{ex,app}$ term to the model-free formalism to take into account the loss of transverse magnetization due to conformational exchange and provided fits to S^2 and $R_{ex,app}$ (M3) and S^2, $\tau_e = \tau_f$, and $R_{ex,app}$ (M4), respectively. Finally, the last model (M5) considered the presence of internal motions slower than τ_f but faster than the overall rotational correlation time of the protein by fitting ${S_f}^2$, S^2, and $\tau_e = \tau_s$. The five dynamic models were fit to the experimental data for each resonance while holding the value of τ_m fixed at the value determined from the trimmed mean of the T_1/T_2 ratio. A grid search was used to obtain initial estimates for the values

of the remaining model parameters by minimizing the χ^2 function defined as

$$\chi^2 = \sum_{i=1}^{N} \Gamma_i = \sum_{i=1}^{N} \sum_{j=1}^{M_i} (R_{ij} - R_{ij}^*)^2/\sigma_{ij}^2 \quad (4)$$

where Γ_i is the sum-squared error for the ith spin, M_i is the number of experimental relaxation parameters, R_{ij} is the jth experimental relaxation parameter for resonance i, R_{ij}^* is the corresponding jth theoretical relaxation parameter calculated from the spectral density model, σ_{ij} is the experimental uncertainty in the jth relaxation parameter for resonance i, and N is the total number of nuclear spins. Statistical properties of the model-free parameters were obtained from Monte Carlo simulations using 600 randomly distributed synthetic data sets.[46] The quality of the fit between the experimental data and theoretical model was assessed for each spin by comparing the optimal value of Γ_i with the $\alpha = 0.05$ critical value of the distribution of Γ_i obtained from the Monte Carlo simulations. Model selection was conducted according to the protocol outlined by Mandel et al.[45] and implemented in FAST-Modelfree. One (M1) and two-parameter (M2 and M3) models were compared by conducting an F-test analysis using a critical α value of 0.2.

Relaxation Dispersion Analysis. Contributions to transverse relaxation rates of conformational exchange were analyzed assuming a two-site exchange process (A ⇔ B) using NESSY.[47] Two models were considered for each spin displaying a nonflat dispersion profile. The first model assumed a slow-limit exchange ($k_{ex} \ll \delta\omega$) between the two sites fitting the relaxation dispersion curves to eq 5

$$R_2^{eff} = R_2^0 + \frac{k_{ex}}{2} - \nu_{CPMG} \cosh^{-1}[D_+ \cosh(\eta_+) - D_- \cos(\eta_-)] \quad (5)$$

where

$$\nu_{CPMG} = (\tau_{cp} + p\omega_{180^\circ})/2$$

$$D_\pm = 1/2[\pm 1 + (\Psi + 2\delta\omega^2)/(\Psi^2 + \xi^2)^{1/2}]$$

$$\eta_\pm = [\pm\Psi + (\Psi^2 + \xi^2)^{1/2}]^{1/2}/(2\sqrt{2}\nu_{CPMG})$$

$$\Psi = k_{ex}^2 - \delta\omega^2$$

$$\xi = -2\delta\omega(p_a k_{ex} - p_b k_{ex})$$

in which ν_{CPMG} is the field strength of CPMG spin−echo pulses, τ_{cp} and $p\omega_{180^\circ}$ are the time delay between consecutive 180° ^{15}N refocusing pulses and the pulse width, respectively, R_2^0 is the transverse relaxation rate constant in the absence of exchange, p_a and p_b are the equilibrium populations at the two sites with $p_a + p_b = 1$, and k_{ex} and $\delta\omega$ are the exchange rate constant and chemical shift difference between the two sites, respectively. The second model considered a fast-limit exchange ($k_{ex} \gg \delta\omega$) between the two sites by fitting the relaxation dispersion curves to eq 6

$$R_2^{eff} = R_2^0 + \frac{\Phi}{k_{ex}}\left[1 - \frac{4\nu_{CPMG}}{k_{ex}} \tanh\left(\frac{k_{ex}}{4\nu_{CPMG}}\right)\right] \quad (6)$$

where $\Phi = p_a p_b \delta\omega^2$. Exchange parameters ($R_2^0$, k_{ex}, p_b, and $\delta\omega$ in model 1 and R_2^0, k_{ex}, and Φ in model 2) were optimized by using the Levenberg−Marquardt algorithm[35] to minimize the least-squares function for each individual amino acid residue

$$\chi^2 = \sum_{i=1}^{N} (R_2^{i,eff,calc} - R_2^{i,eff,exp})^2/\sigma_{R_2^{eff}}^2$$

where i is the index for field strength ν_{CPMG}, σ is the uncertainty in the experimentally measured $R_2^{i,eff,exp}$, and $R_2^{i,calc}$ is the calculated effective transverse relaxation rate constant. Model selection was performed using the Akaike information criteria with second-order correction for small sample size.[48] The uncertainties in the parameters were estimated from 500 Monte Carlo simulations. For a set of residues displaying nearly the same k_{ex} and p_b by the individual fit procedure, a cluster analysis was performed to obtain an estimate of the thermodynamic parameters of exchange.

RESULTS

Resonance Assignments and Chemical Shift Perturbation Mapping. Sequence-specific backbone resonance assignments for apo and holo I-BABP were established using four 3D triple-resonance experiments conducted with uniformly ^{13}C- and ^{15}N-enriched protein at 25 °C, as detailed in Materials and Methods. The assignment of the holo form was conducted at a protein:bile salt molar ratio of 3, using an equimolar mixture of unenriched GCA and GCDA. At this I-BABP:bile salt molar ratio, more than 99.9% of the protein is expected to be in its bound state.[8] Figure 2 displays the 25 °C ^{1}H−^{15}N HSQC spectra of free and doubly ligated I-BABP. Resonance assignment was established for 125 of the 126 non-proline residues of both apo and holo I-BABP. The backbone amide assignments for the two forms are listed in Table S1 of the Supporting Information. The root-mean-square weighted ^{1}HN, ^{15}N, and ^{13}CO chemical shift differences[49] between apo and holo I-BABP were calculated on a per-residue basis and are depicted in Figure 3. The largest perturbations (>6.0 ppm) were observed for residues N96 and H98 in the G−H turn near binding site 1, followed by Y97 and two segments in helix I (D15−L21) and helix II (S24−R32). Additionally, a continuous stretch of residues with above average chemical shift differences was observed for T73−T82 corresponding to the E−F turn and the N-terminal half of β-strand F.

To confirm the position and length of the secondary structure elements under our experimental conditions, a chemical shift index (CSI) analysis was performed using the $^1H_\alpha$, $^{13}C_\alpha$, $^{13}C_\beta$, and ^{13}CO chemical shift values according to Wishart and Sykes.[26] A comparison of the chemical shift-derived secondary structures of apo I-BABP and that of the heterotypic I-BABP:GCA:GCDA (1.0:1.5:1.5) complex is included in Figure S1 of the Supporting Information. As expected, the overall topology of the two forms was the same. The most significant difference between the unligated and doubly ligated protein occurred in the E−F region. Upon ligand binding, β-strand E becomes shorter and is shifted toward the C-terminus, resulting in a longer D−E turn and a shorter E−F turn. Unlike in the case of intestinal fatty acid binding protein, a well-studied member of the intracellular lipid binding protein family, for which NMR spectroscopy measurements have indicated a disordered helix II in the apo state,[50] in I-BABP both α-helices are well-defined in the apo and holo forms of the protein. This is in full agreement with a previous NMR structural investigation

dx.doi.org/10.1021/bi201588q | Biochemistry 2012, 51, 1848−1861

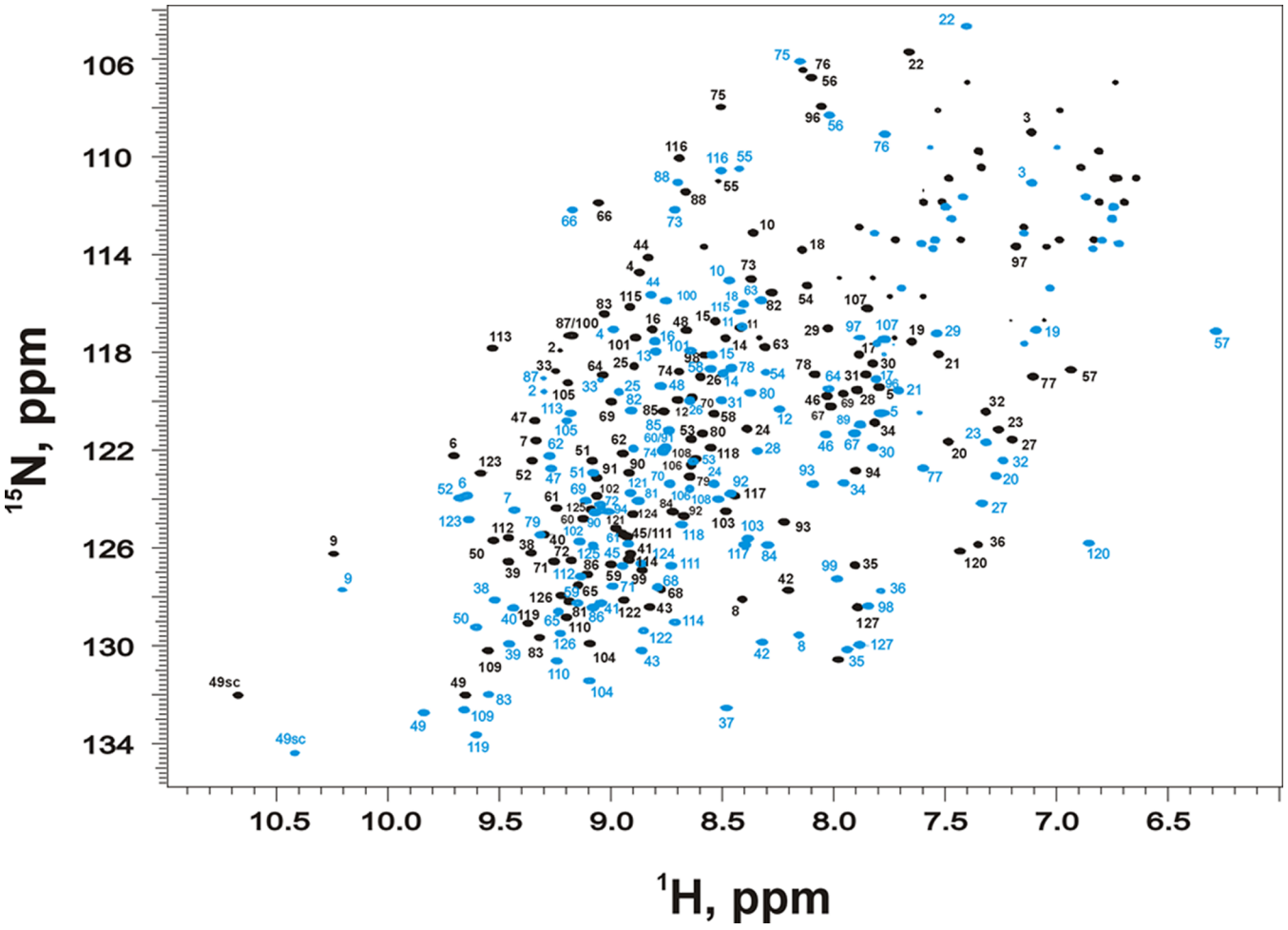

Figure 2. Superposition of gradient- and sensitivity-enhanced 2D ^{1}H−^{15}N heteronuclear single-quantum coherence (HSQC) spectra (600 MHz, 25 °C) of uniformly ^{15}N-enriched apo I-BABP (black) and holo I-BABP complexed with GCA and GCDA at a molar ratio of 1.0:1.5:1.5 (blue). Backbone amide correlations are labeled by residue number according to the assignments described in the text. A full list of backbone ^{1}HN and ^{15}N resonance assignment for the apo protein and the doubly ligated complex is available in the Supporting Information. Resonances in the top right quadrant of the spectra represent side chain NH_2 correlations in asparagine and glutamine residues.

of human I-BABP performed under slightly different pH and temperature conditions.[37]

Amide Hydrogen Exchange Measured by Saturation Transfer. Local unfolding events are known to disrupt backbone hydrogen bonding interactions in proteins, thereby leading to an increased level of exchange with solvent hydrogens.[51,52] To monitor hydrogen exchange rates occurring on the time scale of the longitudinal relaxation rate of amide protons, the relative intensity of ^{1}H−^{15}N correlations collected with and without solvent presaturation during the relaxation delay[53] has been determined for apo and holo I-BABP. Both states of the protein are characterized with below average solvent exchange in the D15−S24 and V27−A31 segments corresponding to helix I, the linker between the two α-helices, and some parts of helix II (data not shown). Interestingly, a drop in peak intensities occurs at the beginning of helix II at residues S25 and D26 in both ligation states, indicating rapid hydrogen exchange. The difference in saturation transfer between the apo and holo forms is displayed in Figure 4 such that a positive difference implies increased protection from hydrogen exchange as a result of bile salt binding. The most significant changes upon ligation occur in the C-terminal half of the protein, in particular at residues Y53, G55, H57−M59, T73−G76, T78−A81, and I114−G116, indicating an increase in the level of protection of the C−D and E−F turns, the N-terminal half of β-strand F, and the I−J turn. Additional diminished solvent exchange is detected in the ligated state at scattered positions, most notably in β-strands G (L90 and N93), H (Q99 and T100), and I (K107 and V111).

Amide ^{15}N NMR Relaxation Parameters. The ^{15}N T_1 and T_2 relaxation times and steady-state $\{^{1}H\}^{15}N$ NOE values were measured on uniformly ^{15}N-enriched I-BABP at two different static magnetic field strengths corresponding to proton Larmor frequencies of 600 and 400 MHz. In apo I-BABP 117, in the doubly-ligated complex 115 of the 126 non-proline residues were included in the analysis. Resonances of low intensity and those showing severe overlap were excluded from the study. Relaxation times and NOEs along the protein sequence obtained at the two static magnetic fields are listed in Tables S2−S5 of the Supporting Information. The average values of parameters are listed in Table 1.

Figure 5 displays the distributions of relaxation parameters as a function of amino acid sequence for the complexed and uncomplexed protein at 600 MHz. It is apparent that there are several regions in the polypeptide chain in both forms where the relaxation parameters differ substantially from their average. For instance, residues S25 and D26 and selected residues between S54 and T58 display T_1 values more than one standard

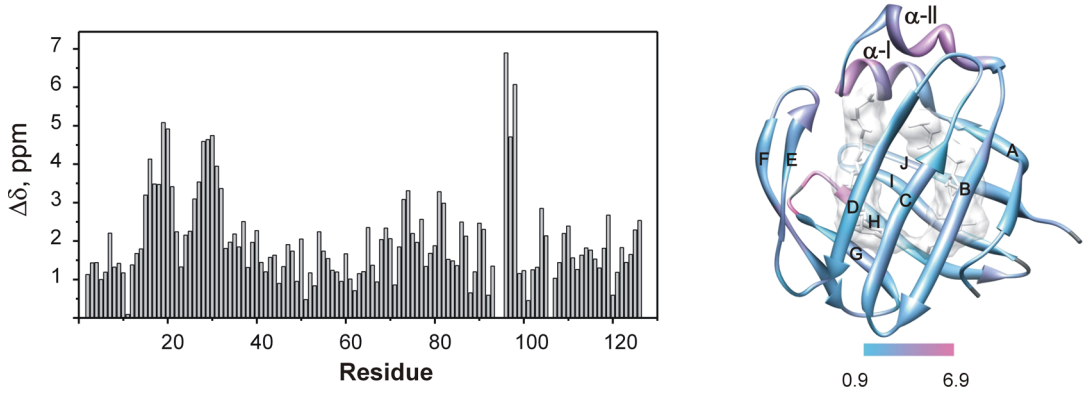

Figure 3. Chemical shift changes upon bile salt binding. Root-mean-square weighted ^{1}HN, ^{15}N, and ^{13}CO chemical shift differences (left) between the apo and holo sates along the amino acid sequence. Combined chemical shift changes were calculated using the equation $\Delta\delta = [(\Delta\delta_{HN})^2 + (w_1\Delta\delta_N)^2 + (w_2\Delta\delta_{CO})^2]$, where w_1 (=0.341) and w_2 (=0.154) are weight factors determined using the BioMagResBank chemical shift database.[49] Chemical shift differences depicted on the left are coded in a cyan-to-pink gradient (right) with the maximal difference as the upper bound and mapped onto the 3D structure of the I-BABP:GCA:GCDA (1.0:1.5:1.5) complex.[10] The images were generated with Chimera 1.5.3.

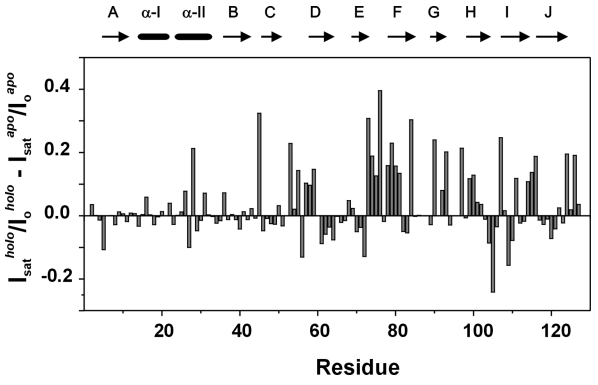

Figure 4. Difference between relative peak intensities of the heterotypic doubly ligated complex [I-BABP:GCA:GCDA (1.0:1.5:1.5)] and apo I-BABP obtained with (I) and without (I_o) presaturation of the solvent resonance as determined at 600 MHz. A positive value denotes an increase in the level of solvent protection upon bile salt binding.

deviation lower than the mean in both the free and the doubly ligated forms. Additionally, in apo I-BABP, the M74−T78 segment exhibits faster than average longitudinal relaxation rates, whereas residues M85, E86, L90, V91, F94, and Y97 tend to show slow ^{15}N T_1 relaxation. In the holo state, above average T_1 values are detected for a number of residues in the T73−K80 and M85−Y97 regions. Similar deviations are observed in the specified regions at 400 MHz, and in general, there is good agreement in the pattern of T_1 relaxation times along the sequence between the two data sets (data not shown). From Figure 5, it is apparent that longitudinal relaxation rates tend to be faster in the complexed state almost along the entire protein sequence. This is most pronounced between residues F34 and N70, spanning β-B, β-C, β-D, and the first few residues of β-E. A very noticeable increase in the T_1 relaxation rate is also found for β-A, part of helix II, and the I-J region at the C-terminal end of the protein upon complexation.

The distribution of transverse relaxation times displays a more uniform pattern along the protein sequence. In the apo protein, T_2 rates faster by more than one standard deviation than their mean are observed at K35, I36, V91, N96, and H98 at both field strengths. At 600 MHz, the list also includes residue E29. These positions correspond to the end of helix II and a linker connecting it to β-B, a residue in β-G, and the G−H turn. Transverse relaxation times reduced to a similar extent are detected in the holo protein for residues R32, N33, and D106 at both field strengths. Segments that show a characteristic change in T_2 upon ligation generally match those exhibiting a similar change in T_1 relaxation (Figure 5). This is most emphasized in the D46−T58 segment corresponding to β-C and the C−D turn, which show a marked increase in the longitudinal and transverse relaxation rates as a result of bile salt binding.

With regard to the steady-state $\{^{1}H\}^{15}N$ NOE parameters, a continuous stretch of higher than average values was detected in helix I between residues Y14 and M18 in the apo protein, whereas the E68−E86 region exhibited a number of residues with lower than average NOEs in the absence and presence of bile salts at both static magnetic field strengths. Residues E68−E86 correspond to a region comprising the β-E and β-F strands where above average T_1 relaxation rates were found in the apo and holo states. Approximately 10% of the residues exhibited NOEs exceeding the theoretical maximum by more than their estimated error at both field strengths, suggesting the presence of highly restricted internal motion at specific positions in the protein. In addition to residues in the terminal region, an extremely low NOE was detected for K77 in the E−F loop at both values of B_o, indicating fast internal motion.

Rotational Diffusion Analysis. The hydrodynamic properties of I-BABP were characterized by rotational diffusion analysis of the T_1 and T_2 relaxation parameters. An initial estimate of the rotational correlation time was obtained from the filtered mean T_1/T_2 ratios according to Kay et al.[36] Residues with T_1/T_2 ratios more or less than one standard deviation from the mean were discarded from the analysis. At 600 MHz (400 MHz), this affected 25 (30) and 14 (10) residues in the apo and holo proteins, respectively. At 600 MHz, the average calculated τ_m was 6.8 ± 0.2 ns for the free protein and 6.7 ± 0.3 ns for the doubly ligated complex, with the given errors representing standard deviations calculated over all residues considered. At 400 MHz, a τ_m of 6.8 ± 0.2 ns was obtained for both protein states.

The principal moment of inertia tensors determined for the apo and holo proteins by PDBinertia were (1.00, 0.86, 0.71) and (1.00, 0.86, 0.76), respectively. The analysis with r2r1_diffusion indicated slightly different $D_{\parallel}/D_{\perp}$ values for the complexed

dx.doi.org/10.1021/bi201588q | Biochemistry 2012, 51, 1848−1861

Table 1. Statistics of Backbone Dynamics of Apo I-BABP and the Heterotypic I-BABP:GCA:GCDA (1.0:1.5:1.5) Ternary Complex

	apo	holo
Relaxation Parameters		
B_o = 14.1 T (ω_H = 600 MHz)		
^{15}N T_1 (ms)	605 ± 38	557 ± 67
^{15}N T_2 (ms)	110 ± 10	103 ± 10
$\{^1H\}^{15}N$ NOE	0.79 ± 0.05	0.77 ± 0.06
$J(0)$ ($\times 10^{-9}$)	2.4 ± 0.2	2.6 ± 0.4
$J(\omega_N)$ ($\times 10^{-10}$)	3.1 ± 0.2	3.4 ± 0.5
$J(\omega_H)$ ($\times 10^{-12}$)	5.5 ± 1.4	6.5 ± 2.0
B_o = 9.4 T (ω_H = 400 MHz)		
^{15}N T_1 (ms)	367 ± 17	355 ± 18
^{15}N T_2 (ms)	117 ± 9	114 ± 9
$\{^1H\}^{15}N$ NOE	0.71 ± 0.06	0.74 ± 0.05
$J(0)$ ($\times 10^{-9}$)	2.4 ± 0.2	2.5 ± 0.3
$J(\omega_N)$ ($\times 10^{-10}$)	5.9 ± 0.3	6.1 ± 0.3
$J(\omega_H)$ ($\times 10^{-11}$)	1.2 ± 0.2	1.1 ± 0.2
Lipari–Szabo Model Parameters		
τ_m (ns)	6.8	6.8
$D_\parallel/D_\perp$	1.1	0.95
S^2 (best of five models)	0.85 ± 0.05	0.88 ± 0.06
no. of residues		
model 1 (S^2)	84	85
model 2 (S^2, τ_e)	11	11
model 3 (S^2, R_{ex})	11	9
model 4 (S^2, τ_e, R_{ex})	–	–
model 5 (S^2, S_f^2, τ_e)	8	9
none of them	3	1
pro/overlap[a]	10	12

[a]In addition to A1 and P95, in the apo state residues Q41, Q45, G87, T100, D106, L108, V111, and I114, in the holo state residues F6, M18, L21, H52, T60, V91, N96, I103, G115, and V117 were excluded from the analysis because of the low signal intensity or severe overlap.

($D_\parallel/D_\perp$ = 0.88) and uncomplexed ($D_\parallel/D_\perp$ = 1.1) states. To take into account the minor effects of anisotropy, we analyzed the relaxation data with the axially symmetric model.

Spectral Density Function Analysis. Spectral densities were calculated for apo I-BABP and the doubly ligated heterotypic complex using eqs 2a–c and are listed in Tables S6 and S7 of the Supporting Information. Deviations from the mean for $J(0)$, $J(\omega_N)$, and $J(\omega_H)$ found at the two different static magnetic fields along the amino acid sequence are displayed schematically in Figure S2 of the Supporting Information for both protein states. The most striking observation is that bile salt binding has a marked effect on slow motions as suggested by a decrease in the number of residues with above average $J(0)$ values, in particular in the C-terminal half of the protein, at both field strengths. Altogether, six specific regions show significant deviations from the mean in their $J(0)$, $J(\omega_N)$, and/or $J(\omega_H)$ values in the apo and/or holo form. (i) The E11–M18 segment is characterized by below average $J(\omega_H)$ values, in particular in the apo protein indicating strong restriction of the backbone N–H vector in helix I. (ii) Throughout the S24–I36 segment corresponding to helix II, above average deviations are found in apo I-BABP for specific residues in all three frequency ranges. Among these, S25 and D26 [(R32 and N33)] are characterized by above average $J(\omega_N)$ [$J(0)$] values in the holo state as well. (iii) An above average $J(\omega_N)$ has also been found for residues in the C–D

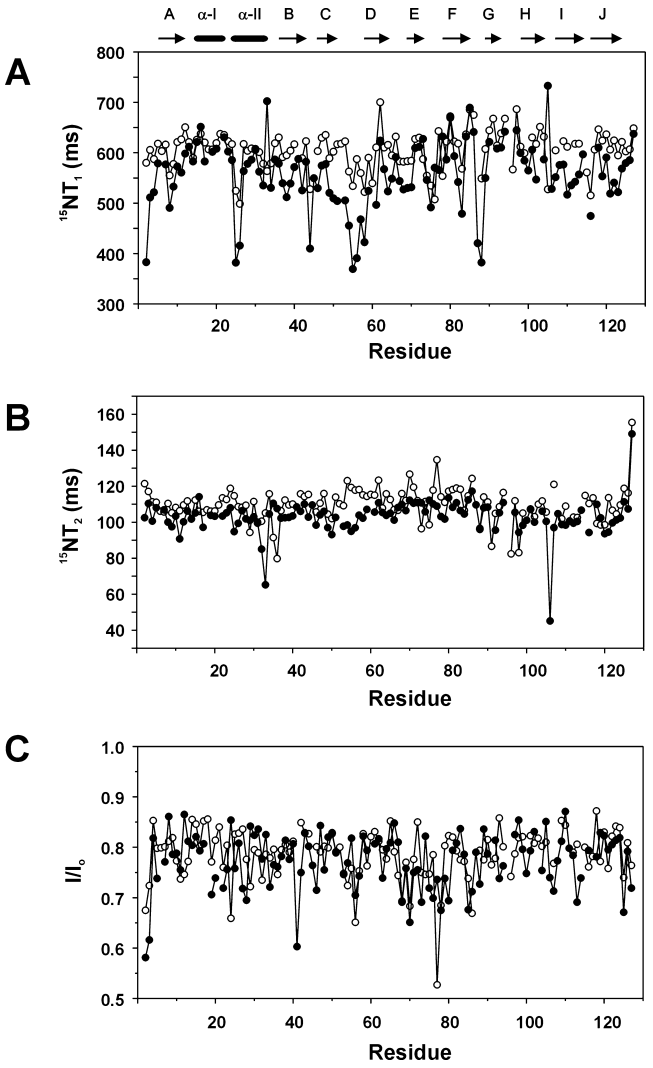

Figure 5. Distribution of the measured ^{15}N T_1 and T_2 relaxation times and $\{^1H\}^{15}N$ NOE parameters at 14.1 T along the amino acid sequence of apo (○) and holo (●) I-BABP. Error bars are not shown for the sake of clarity. The standard deviations of the relaxation parameters are listed in Tables S2 and S3 of the Supporting Information.

turn (e.g., G55, H57, T58, and T60 and S54–T58 in the apo and holo states, respectively). There are also indications of high-frequency motion in the same region manifested in the relaxation behavior of residues S54–G56 in the apo form. (iv) High-frequency motions are also prevalent in β-E and the E–F turn (E68–T78) in apo I-BABP. (v and vi) Finally, the G88–H98 and T118–E120 segments in the apo state are characterized by above average $J(0)$ values accompanied by low values of $J(\omega_N)$ (e.g., V91, F94, and Y97) or $J(\omega_H)$ (T118 and E120), suggesting the presence of slow fluctuations.

To obtain residue-specific information about the amplitude of internal motions present in the two ligation states, spectral densities derived from NMR relaxation data were analyzed in terms of the extended model-free approach as described in Materials and Methods. Generalized order parameters together with effective correlation times for internal motions (τ_e) as well as apparent contributions to transverse relaxation from conformational exchange ($R_{ex,app}$) determined for the free protein and the heterotypic doubly ligated complex are shown in Figure 6. The statistics of backbone dynamics are summarized

dx.doi.org/10.1021/bi201588q | Biochemistry 2012, 51, 1848–1861

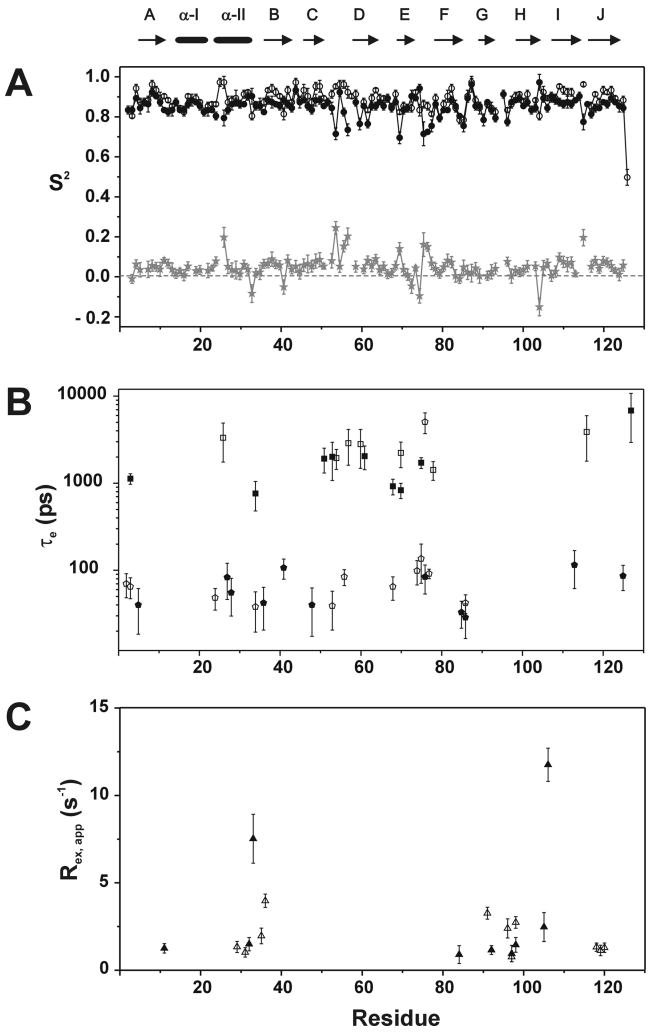

Figure 6. Results of the model-free analysis of the ^{15}N relaxation data obtained at 14.1 T (600 MHz) and 9.4 T (400 MHz). (A) Distribution of the generalized order parameter, S^2, obtained from a fit of the most appropriate representation of the spectral density function along the amino acid sequence of apo (○) and holo (●) I-BABP. Details of model selection are described in the text. The difference $\Delta S^2 = S_{holo}{}^2 - S_{apo}{}^2$ is colored gray. (B) Internal correlation times shown on a logarithmic scale. Values of τ_e of <200 ps are represented by diamonds, whereas values of 200 ps < τ_e < τ_m are shown as squares. Empty and filled symbols correspond to apo and holo samples, respectively. (C) Apparent contributions to transverse relaxation from chemical exchange in apo I-BABP (△) and the heterotypic I-BABP:GCA:GCDA (1.0:1.5:1.5) complex (▲).

in Table 1. For both forms of the protein, ~70% of the residues were fit by the simplest model-free formalism using S^2 alone. In the apo state 19 and in the holo state 20 residues required the inclusion of an effective correlation time for internal motions. Among these, in the unbound form eight residues and in the ligated state nine residues were fit by the two-time scale spectral density function (Figure 6B). With the exception of S68 (τ_e < 200 ps), D26, T60, and N70 (200 ps < τ_e) (apo), V27, I28, Q41, T48, and T113 (τ_e < 200 ps), and N61 and N70 (200 ps < τ_e) (holo), the residues exhibiting picosecond to nanosecond mobility for which τ_e < τ_m were located either in loop regions or at the termini of secondary structure elements. Among the loops, in the apo form, the C−D and E−F loops appeared to be the most affected by fast backbone motion. In apo I-BABP eleven residues and in the doubly ligated complex nine residues required an apparent conformational exchange term to fit their relaxation parameters (Figure 6C). In particular in the free state, most of these residues were clustered into three specific regions such as helix II and a linker connecting it to β-strand B (E29, A31, K35, and I36) as well as two short segments in the G−H loop region (N96−H98) and on β-strand J (T118−E120). Among the listed regions, helix II (R32 and N33) and the G−H loop indicated signs of a microsecond to millisecond motion also in the holo state. The contribution of conformational exchange to transverse relaxation has also been estimated from the field dependence of $T_2^{-1} - T_1^{-1}/2$ (ref 54), and in particular in the apo state, there was a good agreement between the two methods when identifying residues suspected to undergo a conformational exchange (data not shown).

From a joint analysis of the 600 and 400 MHz relaxation data, the average order parameters obtained for the apo and holo states were 0.85 ± 0.05 and 0.88 ± 0.06, respectively. The average S^2 values for various secondary structure elements are listed in Table 2. A slight increase was found in $\langle S^2 \rangle$ throughout the protein sequence indicative of a small decrease in the backbone picosecond to nanosecond mobility upon formation of the complex. The largest increase (≥0.05) in the average order parameter occurred for β-C, β-D, and β-J, whereas the smallest increase (≤0.02) was detected for β-G, β-E, and helix I. Upon inspection of the linker and turn regions, the largest increase in $\langle S^2 \rangle$ has been found in the C−D and I−J turns as a result of bile salt binding. On the other hand, a decrease of >0.03 was observed in $\langle S^2 \rangle$ for the F−G turn. In the apo state three residues (S25, T58, and A127) and in the holo state one residue (F2) could not be fit to any of the five models. The $S_{holo}{}^2 - S_{apo}{}^2$ differences mapped to the ribbon representation of the mean coordinates of the heterotypic I-BABP:GCA:GCDA (1.0:1.5:1.5) complex are shown in Figure 7. The full list of motional parameters obtained from the model-free analysis for apo and holo I-BABP is given in Tables S8 and S9 of the Supporting Information.

Relaxation Dispersion Analysis. The need for an apparent chemical exchange term, $R_{ex,app}$, to achieve an adequate fit of the ^{15}N relaxation NMR data when using the Lipari−Szabo model-free formalism suggested that conformational motions on the microsecond to millisecond time scale may play a significant role in the mechanism of bile salt binding. For accurate characterization of the conformational motion on this time scale, a series of Carr−Purcell−Meiboom−Gill (CPMG) relaxation dispersion experiments[31,32,55] were conducted on uniformly 80% ^{2}H- and 99% ^{15}N-enriched apo and holo I-BABP.

In the apo state, 30 of the assignable 117 backbone amide groups had a detectable R_{ex}. Representative transverse relaxation dispersions as a function of CPMG field strength are plotted in Figure 8. The residues sensing an exchange process on the micro- to millisecond time scale in the uncomplexed state were predominantly located in the C-terminal half of the protein (Figure 9), more specifically in segments of β-strands E (S69−T73), F (G76−T82), G (V91−N93), H (N96−Q99), I (S112−G116), and J (R121). In addition, R_{ex} was detected in the C−D loop region and at a single position (K35) at the connection of helix II and β-strand B. In contrast, in the holo protein, all of the residues except for F2, S25, and T78 exhibited a flat relaxation dispersion profile, indicating the cessation of slow conformational fluctuations upon ligand binding.

dx.doi.org/10.1021/bi201588q | Biochemistry 2012, 51, 1848−1861

Table 2. Average Order Parameter Values for Secondary Structure Elements

	apo I-BABP		holo I-BABP[a]	
	residues	$\langle S^2 \rangle$	residues	$\langle S^2 \rangle$
helix				
α-I	14–22	0.85 (0.02)	14–20	0.87 (0.03)
α-II	24–34	0.85 (0.04)	24–33	0.89 (0.05)
strand				
β-A	5–12	0.86 (0.03)	5–12	0.90 (0.03)
β-B	36–41	0.86 (0.02)	36–43	0.90 (0.04)
β-C	46–51	0.86 (0.02)	46–51	0.91 (0.03)
β-D	59–64	0.82 (0.05)	58–64	0.89 (0.03)
β-E	67–72	0.83 (0.07)	69–73	0.85 (0.03)
β-F	78–86[b]	0.81 (0.05)	78–85	0.85 (0.06)
β-G	89–93	0.84 (0.02)	89–93	0.86 (0.02)
β-H	97–102	0.85 (0.04)	98–104	0.89 (0.02)
β-I	107–114	0.87 (0.02)	107–114	0.91 (0.03)
β-J	117–124	0.85 (0.02)	117–124	0.90 (0.03)
linker				
β-A/α-I	13	0.83 (0.00)	13	0.82 (0.00)
α-II/β-B	35	0.85 (0.00)	34 and 35	0.86 (0.00)
reverse turn				
α-I/α-II	23	0.83 (0.00)	21–23	0.86 (0.01)
β-B/β-C	42–45	0.88 (0.04)	44 and 45	0.87 (0.06)
β-C/β-D	52–58	0.82 (0.08)	52–57	0.94 (0.03)
β-D/β-E	65 and 66	0.86 (0.02)	65–68	0.88 (0.02)
β-E/β-F	73–77	0.83 (0.11)	74–77	0.87 (0.04)
β-F/β-G	87 and 88	0.92 (0.00)	86–88	0.88 (0.09)
β-G/β-H	94–96	0.85 (0.09)	94–97	0.83 (0.01)
β-H/β-I	103–106	0.88 (0.06)	105 and 106	0.86 (0.09)
β-I/β-J	115 and 116	0.83 (0.09)	115 and 116	0.96 (0.00)

[a]Human I-BABP was complexed with an equimolar mixture of GCA and GCDA at a protein bile salt molar ratio of 1.0:1.5:1.5. [b]In the uncomplexed protein, a break occurred in β-F between T82 and V83. Secondary structure elements are defined by the consensus chemical shift index according to Wishart and Sykes.[26]

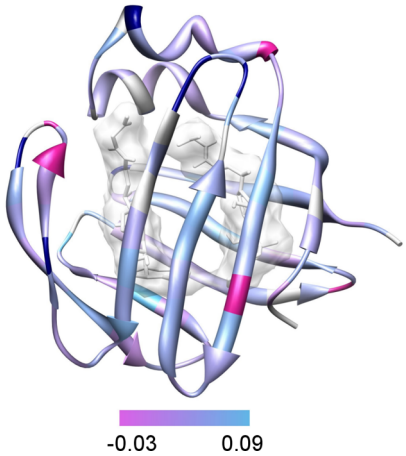

Figure 7. Differences in the generalized order parameter occurring upon bile salt binding ($\Delta S^2 = S_{holo}^2 - S_{apo}^2$) are mapped on the ribbon diagram of the mean coordinates of the heterotypic I-BABP:GCA:GCDA (1.0:1.5:1.5) complex[10] and coded in a pink-to-cyan gradient. Residues exhibiting a ΔS^2 below or above the designated limits are colored deep pink or blue, respectively.

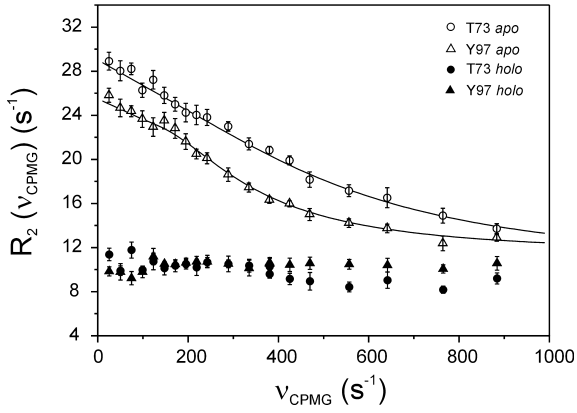

Figure 8. Transverse relaxation dispersions of the backbone ^{15}N nuclei of T73 (circles) and Y97 (triangles) in apo human I-BABP (empty symbols) and the heterotypic I-BABP:GCA:GCDA (1.0:1.5:1.5) complex (filled symbols) as a function of CPMG B_1 field strength. The experiments were conducted at 25 °C at a static magnetic field strength of 14.1 T. Error bars are standard deviations derived from duplicate measurements. Solid lines represent best-fit curves generated by NESSY[47] with an individual fit procedure.

The nonflat dispersion curves observed for the apo state were individually fit assuming a two-state exchange process between a ground state (A) and an excited state (B) as described in Materials and Methods. For the 30 residues indicated in Figure 9, the average R_{ex} value was found to be 5.7 ± 5.0 s^{-1}. The average individual exchange constant ($k_{ex} = k_{A\rightarrow B} + k_{B\rightarrow A}$) was 400 ± 381 s^{-1}. Two residues (S69 and V92) had a small k_{ex} value, which was more than one standard deviation below the mean ($k_{ex} < 20$ s^{-1}). In contrast, four residues (H98, M59, A81, and S112) exhibited an exceptionally high exchange constant

dx.doi.org/10.1021/bi201588q | Biochemistry 2012, 51, 1848–1861

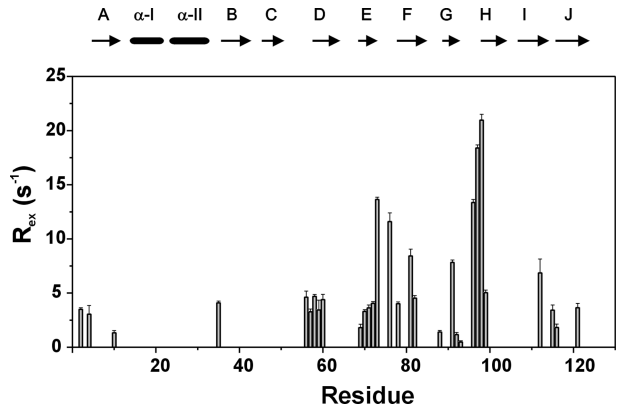

Figure 9. Histograms of the contribution to transverse relaxation from conformational exchange as derived from CPMG relaxation dispersion measurements on apo human I-BABP at 25 °C at a static magnetic field strength of 14.1 T. The R_{ex} values were determined assuming a two-state exchange process between a ground state and an excited state using NESSY.[47]

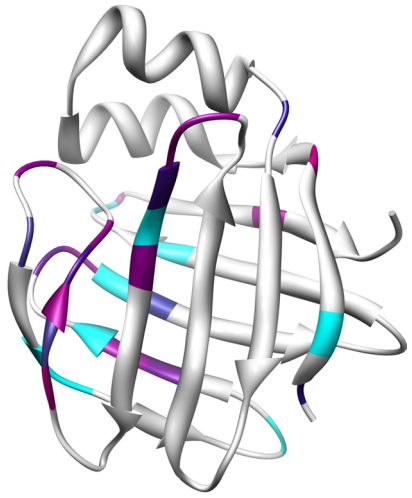

Figure 10. Backbone ^{15}N chemical shift modulation as a result of conformational exchange on the microsecond to millisecond time scale as determined from CPMG relaxation dispersion experiments mapped on the ribbon representation of the mean coordinates of apo human I-BABP (PDB entry 1O1U[37]). Differences in chemical shifts were determined from individual fits assuming a two-state exchange process between a ground state and an excited state and are coded in a blue-to-pink gradient according to the ratio $\Delta\delta_i/\Delta\delta_{max}$, where $\Delta\delta_i$ is the chemical shift difference of residue i and $\Delta\delta_{max}$ = 2.2 ppm. Residues undergoing a fast-limit exchange ($k_{ex} > \delta\omega$) are colored cyan. Residues exhibiting a flat dispersion profile or with no available data are colored gray. The figure was generated using Chimera 1.5.3.

(k_{ex} > 800 s^{-1}). Altogether, among the 30 affected residues, nine showed a fast-limit exchange (eq 6), whereas 21 appeared to undergo a slow-limit exchange (eq 5). Ideally, the latter allows us to obtain not only kinetic but also thermodynamic and structural information about the exchange process. On the basis of individual fit analysis of the residues undergoing a slow-limit exchange, an average p_b value of 0.08 ± 0.05 was obtained for the excited-state population(s). The chemical shift differences found for individual ^{15}N spins mapped to the ribbon diagram of the mean coordinates of apo I-BABP (PDB entry 1O1U[37]) are shown in Figure 10. The differences were in general less than 2.2 ppm, and the largest $\delta\omega$ values were found for residues G56, T60, G76, G116, and V92, located in the C−D, E−F, and I−J loop regions and on β-strand G. We emphasize that as CPMG curves have been obtained at only a single static magnetic field strength, the values listed above should only be considered as crude estimates.

DISCUSSION

Flexibility and function are closely related in proteins. Internal motions with different time scales, amplitudes, and intensities are superimposed onto each other in a protein molecule, most of them with specific functional importance. To obtain a mechanistic view of protein action, an atomic scale understanding of the dynamic processes is necessary.

In the enterohepatic circulation of bile salts, human I-BABP takes up bile salts at the apical membrane of enterocytes and carries them to the basolateral ileal membrane where they are secreted into portal capillaries and transported back to the liver. Intracellular trafficking and membrane targeting of bile salts need sophisticated regulation. To fulfill its function, I-BABP is endowed with remarkable properties. In particular, positive binding cooperativity[7,8,10] in combination with site selectivity[9] allows it to function as a highly efficient sponge against dangerously high levels[56] of structurally diverse bile salts in enterocytes. Previous stopped-flow kinetic measurements have revealed a slow conformational change (milliseconds) in I-BABP related to binding cooperativity and raised the possibility of a separate conformational fluctuation (microseconds to milliseconds) in the apo state itself.[11] As a first step in sorting out the various time scale fluctuations in the protein and relating the macroscopic kinetic data to residue-specific dynamic events, in this study we have characterized the internal motion of backbone N−H vectors in apo I-BABP and in the heterotypic doubly ligated I-BABP:GCA:GCDA (1.0:1.5:1.5) complex using ^{15}N NMR relaxation techniques.

Our data have shown a fairly rigid backbone dynamics on the pico- to nanosecond time scale for both apo and holo I-BABP. A slight decrease in N−H bond vector mobility seems to exist upon bile salt binding, with the most significant changes occurring in the C−D loop in the vicinity of the putative portal region. A smaller increase in S^2 occurs throughout the protein upon ligation. We note that such a small increase in S^2 may in theory also arise from a small increase in the overall correlation time of the molecule. However, on the basis of both the filtered mean average of the T_1/T_2 ratios at both static field strengths and the outcome of the model-free analysis, no increase is indicated in τ_m upon ligand binding. Thus, it seems more likely that the slight elevation of S^2 we observe as a result of bile salt binding in fact arises from a slight decrease in N−H bond vector mobility. Assuming a restricted diffusion in a cone motional model,[40,57] the decrease can be estimated to be about ∼2−3°. Such freezing of motion upon ligand binding has been reported for a number of other proteins such as chorismate mutase,[58] HIV protease,[59] RNase A,[60] and RNase H[61] and suggests that backbone configurational entropy is not a major source of stabilization in the formation of the I-BABP:bile salt complex.

While the effect of ligation on the picosecond to nanosecond dynamics is clearly minor, relaxation dispersion analysis of CPMG NMR experiments have revealed marked differences in the microsecond to millisecond conformational fluctuations between apo and holo I-BABP. In the unligated form, nearly 25% of the residues have been found to undergo a conformational exchange process, whereas in the doubly ligated complex, essentially all of the residues exhibited a flat relaxation

dx.doi.org/10.1021/bi201588q | Biochemistry 2012, 51, 1848−1861

dispersion curve. The affected residues are mainly localized in the C-terminal half of the apo protein, forming an almost continuous network of fluctuations extending from β-strand J to the E−F side of the protein. On the basis of a field-dependent analysis of ^{15}N NMR relaxation data, a similarly extensive network of microsecond to millisecond fluctuations has been detected in the C-terminal half of apo chicken liver bile acid binding protein,[15] and by CPMG relaxation dispersion analysis, an even more inclusive conformational exchange has been uncovered in the unligated forms of CRBP I and II.[14] Similar to the situation in human I-BABP, the detected millisecond time scale fluctuations cease upon ligand binding in both proteins. Approximately two-thirds of the residues with a detectable R_{ex} in the CPMG experiments in apo I-BABP exhibited similar k_{ex} rates, allowing us to subject them to a global two-state exchange process. This resulted in a k_{ex} of 477 ± 82 s^{-1} that is somewhat higher than the average obtained from individual fits and a somewhat smaller p_b value of 0.07 ± 0.03 s^{-1}. When these are converted into forward and reverse rate constants of the A ↔ B exchange process, where A is the ground state and B is the excited state, a $k_{A\rightarrow B}$ of 33 ± 15 s^{-1} and a $k_{B\rightarrow A}$ of 444 ± 78 s^{-1} are obtained, corresponding to a Gibbs free energy (ΔG_{BA}) of ∼1.5 ± 0.3 kcal. Although the parameters listed above seem reasonable, we emphasize that as CPMG experiments have been conducted at only a single B_o field strength, the thermodynamic parameters for the exchange process ought to be considered as crude estimates. Also, the fact that the ∼10 remaining residues could only be fit by a substantially smaller or greater k_{ex} indicates that there are likely, not a single excited state, but rather a manifold of low populated excited-state conformations in the unligated protein.

Plotting the R_{ex} values derived from the relaxation dispersion analysis as a function of the amino acid sequence (Figure 9) and mapping the chemical shift changes to the ribbon diagram of the mean coordinates of apo I-BABP (Figure 10) show that the regions most affected by the exchange process are the E−F and G−H regions. It is worth noting that the latter corresponds to a segment in which bile salt binding was accompanied by an exceptionally large chemical shift change (Figure 3). Such marked changes in the chemical environment should be indications of charge redistributions in the region caused by hydrogen bond or salt bridge formation. In fact, H98 is a conserved residue among bile acid binding proteins and in cl-BABP has been implicated in the modulation of a microsecond to millisecond time scale motion associated with an opening−closing motion of the protein and mediating ligand binding by changing its protonation state.[15,62] As evidenced by NMR line shape and relaxation dispersion analysis performed on wild-type and disulfide bridge-containing (T91C) cl-BABP analogues,[63,64] the slow motion communicated from H98 to the E−F loop has been found to be associated with site selectivity of bile salt binding. In the human analogue, NMR spectroscopic and calorimetric studies of a point mutation in the region (Q99A) have indicated no apparent role of Q99 in site selectivity; however, together with E110, N61 and W49 have been shown to be part of a hydrogen bonding network, which by mediating the communication between the two binding sites plays a key role in positive binding cooperativity.[10] The overlap between the region indicated by the current relaxation dispersion analysis to undergo slow microsecond to millisecond fluctuations in apo I-BABP and the previously indicated H-bonding network raises the possibility of a potential role of conformational fluctuations occurring in the free protein not only in ligand entry but also in positive cooperativity of bile salt binding.

Unlike in cl-BABP, the network of microsecond to millisecond fluctuations detected in apo I-BABP by CPMG experiments includes the C−D loop and a short linker connecting helix II to its neighboring β-strand. We note that model-free analysis of the ^{15}N T_1, T_2, and $\{^1H\}^{15}N$ NOE relaxation data has shown a contribution of microsecond to millisecond fluctuations to transverse relaxation in the helical region in the apo (E29 and A31) and holo (E11, R32, and N33) forms. Thus, there is a possibility that some of the residues in the helical region not detected in relaxation dispersion measurements might undergo conformational exchange on time scales outside of the ∼50 μs to 5 ms detection window of the CPMG experiments. Temperature-dependent relaxation dispersion and $T_{1\rho}$ experiments to assess faster motions are in progress to clarify this possibility. In particular, the involvement of the helical region in ligand entry and release has previously been indicated for various fatty acid binding proteins[12,13,50,65,66] and CRBPs.[14] According to the so-called dynamic portal hypothesis, a localized region of backbone disorder exists in the helical cap in apo I-FABP, which by acting as a flexible gate permits the entry of ligand. By a series of interactions between helix II and the neighboring C−D turn, fatty acid binding stabilizes the protein and shifts the order−disorder equilibrium toward the ordered, closed state. Increased picosecond fluctuations have also been observed in the helical region of apo cl-BABP.[15] In contrast, in CRBP I and II, although no signs of increased picosecond mobility in the absence of retinol have been detected, CPMG experiments have shown a significant conformational flexibility of the helical region on the millisecond time scale.[14] Moreover, in apo CRBP II, the increased values of conformational exchange rates and dynamic ^{15}N chemical shift differences observed in helix II are parallel with a structural disorder in the region.[14] Unlike in I-FABP and cl-BABP, according to our data, the helical segments of I-BABP appear to be rigid on the picosecond to nanosecond time scale in both ligation states. We note that as opposed to apo I-FABP[50] and CRBP II,[14] our chemical shift analysis and saturation transfer data show that in I-BABP both helices are well-defined in both states of the protein. These observations raise the possibility that unlike in a number of FABPs and CRBP II, the helical cap in human I-BABP may not have such a key role in ligand entry and release. One possibility would be the existence of a different portal region. On the basis of the shortened β-strands G and H found in BABPs in comparison with FABPs, a second portal for ligand entry and exit has been proposed and indicated by NMR structure determination of apo porcine I-BABP in the past.[67] However, we should note that the dynamic behavior of porcine I-BABP[68] differs significantly from that of the human analogue on both fast and slow time scales. Intriguingly, while point mutagenesis and deletion of the helical domain of various fatty acid binding proteins altered their interactions with lipid bi- and monolayers, underlying the helical domain as a key determinant in ligand release,[65,66] for bile acid binding proteins, a different antiportal region localized at the bottom of the β-barrel has been indicated.[69]

Previously, on the basis of stopped-flow fluorescence data, we have hypothesized a conformational selection model as a possible mechanism of bile salt binding to human I-BABP.[11] According to this scheme, there are two distinct conformational states of the protein, an open (T) state and a closed (R) state, from which T is thermodynamically favored in the

absence of ligands, but upon ligand binding, the equilibrium is shifted toward the R state. The transition between the open and closed forms of the protein is thought to be realized after the occupation of both binding sites and is a result of the stronger affinity of the R state for the ligands. The dramatic cessation of conformational exchange on the microsecond to millisecond time scale upon ligand binding, as shown by the relaxation dispersion analysis of apo I-BABP and the heterotypic I-BABP:GCA:GCDA complex, may be the manifestation of a stabilization of the closed state occurring upon ligand binding and might be an explanation for the stronger affinity of the R state for the ligands. Further mutagenesis and NMR structural work in combination with dynamic studies assessing additional time scales should give us more insight into the functional role of slow dynamics present in apo I-BABP, in particular into its possible connection with positive cooperativity and site selectivity of human I-BABP−bile salt recognition.

■ ASSOCIATED CONTENT

Supporting Information

Lists of ^{1}H and ^{15}N resonance assignments, relaxation and motional parameters obtained for apo human I-BABP and the heterotypic I-BABP:GCA:GCDA complex, results of secondary structure analysis, and a comparison of the model-free analysis obtained for the holo complex using two different sets of coordinates. This material is available free of charge via the Internet at http://pubs.acs.org.

■ AUTHOR INFORMATION

Corresponding Author

*E-mail: toke@chemres.hu. Telephone: +36-1-438-4141/289. Fax: +36-1-438-1145.

Funding

Research was supported by grants from the Hungarian Research Fund (OTKA) F68326, the Hungarian GVOP-3.2.1-2004-04-0210/3.0 project, and by CRC-HAS-2009 Nano-transport.

Notes

The authors declare no competing financial interest.

■ ACKNOWLEDGMENTS

We thank Dr. Gregory DeKoster and Prof. David Cistola for the coordinates of the heterotypic doubly ligated I-BABP complex and the pMON5840 plasmid, Prof. Julianna Kardos for helping in the establishment of the Protein Expression Facility, and Prof. Gábor Pálinkás for his support and stimulating research environment at the Chemical Research Center of the Hungarian Academy of Sciences.

■ ABBREVIATIONS

CPMG, Carr−Purcell−Meiboom−Gill; CRBP, cellular retinol binding protein; FABP, fatty acid binding protein; GCA, glycocholic acid; GCDA, glycochenodeoxycholic acid; HSQC, heteronuclear single-quantum coherence; ITC, isothermal titration calorimetry; I-BABP, ileal bile acid binding protein; NMR, nuclear magnetic resonance.

■ REFERENCES

(1) Danielsson, H., and Sjovall, J. (1985) *Sterols and bile acids*, Vol. *12*, Elsevier, Amsterdam.

(2) Makishima, M., Okamoto, A. Y., Repa, J. J., Tu, H., Learned, R. M., Luk, A., Hull, M. V., Lustig, K. D., Mangelsdorf, D. J., and Shan, B. (1999) Identification of a nuclear receptor for bile acids. *Science 284*, 1362−1365.

(3) Houten, S. M., Watanabe, M., and Auwerx, J. (2006) Endocrine functions of bile acids. *EMBO J. 25*, 1419−1425.

(4) Small, D. M., Dowling, R. H., and Redinger, R. N. (1972) The enterohepatic circulation of bile salts. *Arch. Intern. Med. 130*, 552−573.

(5) Banaszak, L., Winter, N., Xu, Z., Bernlohr, D. A., Cowan, S., and Jones, T. A. (1994) Lipid-binding proteins: A family of fatty acid and retinoid transport proteins. *Adv. Protein Chem. 45*, 89−151.

(6) Veerkamp, J. H., and Maatman, R. G. (1995) Cytoplasmic fatty acid-binding proteins: Their structure and genes. *Prog. Lipid Res. 34*, 17−52.

(7) Tochtrop, G. P., Richter, K., Tang, C., Toner, J. J., Covey, D. F., and Cistola, D. P. (2002) Energetics by NMR: Site-specific binding in a positively cooperative system. *Proc. Natl. Acad. Sci. U.S.A. 99*, 1847−1852.

(8) Tochtrop, G. P., Bruns, J. M., Tang, C., Covey, D. F, and Cistola, D. P. (2003) Steroid ring hydroxylation patterns govern cooperativity in human bile acid binding protein. *Biochemistry 42*, 11561−11567.

(9) Tochtrop, G. P., DeKoster, G. T., Covey, D. F., and Cistola, D. P. (2004) A single hydroxyl group governs ligand site selectivity in human ileal bile acid binding protein. *J. Am. Chem. Soc. 126*, 11024−11029.

(10) Toke, O., Monsey, J. D., DeKoster, G. T., Tochtrop, G. P., Tang, C., and Cistola, D. P. (2006) Determinants of cooperativity and site-selectivity in human ileal bile acid-binding protein. *Biochemistry 45*, 727−737.

(11) Toke, O., Monsey, J. D., and Cistola, D. P. (2007) Kinetic mechanism of ligand binding in human ileal bile acid binding protein as determined by stopped-flow fluorescence analysis. *Biochemistry 46*, 5427−5436.

(12) Cistola, D. P., Kim, K., Rogl, H., and Frieden, C. (1996) Fatty acid interactions with a helix-less variant of intestinal fatty acid-binding protein. *Biochemistry 35*, 7559−7565.

(13) Hodsdon, M. E., and Cistola, D. P. (1997) Ligand binding alters the backbone mobility of intestinal fatty acid-binding protein as monitored by ^{15}N NMR relaxation and ^{1}H exchange. *Biochemistry 36*, 2278−2290.

(14) Lu, J., Cistola, D. P., and Li, E. (2003) Two homologous rat cellular retinol-binding proteins differ in local conformational flexibility. *J. Mol. Biol. 330*, 799−812.

(15) Ragona, L., Catalano, M., Luppi, M., Cicero, D., Eliseo, T., Foote, J., Fogolari, F., Zetta, L., and Molinari, H. (2006) NMR dynamic studies suggest that allosteric activation regulates ligand binding in chicken liver bile acid-binding protein. *J. Biol. Chem. 281*, 9697−9709.

(16) Li, E., Locke, B., Yang, N. C., Ong, D. E., and Gordon, J. I. (1987) Characterization of rat cellular retinol-binding protein II expressed in *Escherichia coli*. *J. Biol. Chem. 262*, 13773−13779.

(17) Pace, C. N., Vajdos, F., Fee, L., Grimsley, G., and Gray, T. (1995) How to measure and predict the molar absorption coefficient of a protein. *Protein Sci. 4*, 2411−2423.

(18) Wittekind, M., and Mueller, L. (1993) HNCACB, a high sensitivity 3D NMR experiment to correlate amide-proton and nitrogen resonances with the α- and β-carbon resonances in proteins. *J. Magn. Reson., Ser. B 101*, 201−205.

(19) Muhandiram, D. R., and Kay, L. E. (1994) Gradient-enhanced triple-resonance three-dimensional NMR experiments with improved sensitivity. *J. Magn. Reson., Ser. B 103*, 203−216.

(20) Kay, L. E., Xu, G. Y., and Yamazaki, T. (1994) Enhanced-sensitivity triple-resonance spectroscopy with minimal H_2O saturation. *J. Magn. Reson., Ser. A 109*, 129−133.

(21) Grzesiek, S., and Bax, A. (1992) Correlating backbone amide and side chain resonances in larger proteins by multiple relayed triple resonance NMR. *J. Am. Chem. Soc. 114*, 6291−6293.

(22) Ikura, M., Kay, L. E., and Bax, A. (1990) A novel approach for sequential assignment of proton, carbon-13, and nitrogen-15 spectra of

larger proteins: Heteronuclear triple-resonance three-dimensional NMR spectroscopy. Application to calmodulin. *Biochemistry 29*, 4659−4667.
(23) Grzesiek, S., and Bax, A. (1992) Improved 3D triple-resonance NMR techniques applied to a 31 kDa protein. *J. Magn. Reson. 96*, 432−440.
(24) Powers, R., Gronenborn, A. M., Clore, M., and Bax, A. (1991) Three-dimensional triple-resonance NMR of $^{13}C/^{15}N$-enriched proteins using constant-time evolution. *J. Magn. Reson. 94*, 209−213.
(25) Markley, J. L., Bax, A., Arata, Y., Hilbers, C. W., Kaptein, R., Sykes, B. D., Wright, P. E., and Wüthrich, K. (1998) Recommendations for the presentation of NMR structures of proteins and nucleic acids. *Pure Appl. Chem. 70*, 117−142.
(26) Wishart, D. S., and Sykes, B. D. (1994) The ^{13}C chemical shift index: A simple method for the identification of protein secondary structure using chemical shift data. *J. Biomol. NMR 4*, 171−180.
(27) Kay, L. E., Keifer, P., and Saarinen, T. (1992) Pure absorption gradient enhanced heteronuclear single quantum correlation spectroscopy with improved sensitivity. *J. Am. Chem. Soc. 114*, 10663−10665.
(28) Kay, L., Nicholson, L., Delaglio, F., Bax, A., and Torchia, D. (1992) Pulse sequences for removal of the effects of cross-correlation between dipolar and chemical-shift anisotropy relaxation mechanisms on the measurement of heteronuclear T1 and T2 values in proteins. *J. Magn. Reson. 97*, 359−375.
(29) Farrow, N. A., Muhandiram, R., Singer, A. U., Pascal, S. M., Kay, C. M., Gish, G., Shoelson, S. E., Pawson, T., Forman-Kay, J. D., and Kay, L. E. (1994) Backbone dynamics of a free and phosphopeptide-complexed Src homology 2 domain studied by ^{15}N NMR relaxation. *Biochemistry 33*, 5984−6003.
(30) Markley, J. L., Horsley, W. J., and Klein, M. P. (1971) Spin-lattice relaxation measurements in slowly relaxing complex spectra. *J. Chem. Phys. 55*, 3604−3605.
(31) Loria, J. P., Rance, M., and Palmer, A. G. III (1999) A relaxation-compensated Carr-Purcell-Meiboom-Gill sequence for characterizing chemical exchange by NMR spectroscopy. *J. Am. Chem. Soc. 121*, 2331−2332.
(32) Tollinger, M., Skrynnikov, N. R., Mulder, F. A. A., Forman-Kay, J. D., and Kay, L. E. (2001) Slow dynamics of folded and unfolded states of an SH3 domain. *J. Am. Chem. Soc. 123*, 11341−11352.
(33) Mulder, F. A., Skrynnikov, N. R., Hon, B., Dahlquist, F. W., and Kay, L. E. (2001) Measurement of slow (micros-ms) time scale dynamics in protein side chains by ^{15}N relaxation dispersion NMR spectroscopy: Application to Asn and Gln residues in a cavity mutant of T4 lysozyme. *J. Am. Chem. Soc. 123*, 967−975.
(34) Goddard, T. D., and Kneller, D. G. (2009) *SPARKY 3*, University of California, San Francisco.
(35) Levenberg, K. (1944) A method for the solution of certain non-linear problems in least squares. *Q. Appl. Math. 2*, 164−168.
(36) Kay, L. E., Torchia, D. A., and Bax, A. (1989) Backbone dynamics of proteins as studied by ^{15}N inverse detected heteronuclear NMR spectroscopy: Application to *Staphylococcal nuclease*. *Biochemistry 28*, 8972−8979.
(37) Kurz, M., Brachvogel, V., Matter, H., Stengelin, S., Thüring, H., and Kramer, W. (2003) Insights into the bile acid transportation system: The human ileal lipid-binding protein-cholyltaurine complex and its comparison with homologous structures. *Proteins 50*, 312−328.
(38) Abragam, A. (1961) *Principles of Nuclear Magnetism*, Clraendon Press, Oxford, U.K.
(39) Case, D. A. (1999) Calculations of NMR dipolar coupling strengths in model peptides. *J. Biomol. NMR 15*, 95−102.
(40) Lipari, G., and Szabo, A. (1982) Model-free approach to the interpretation of nuclear magnetic resonance relaxation in macromolecules. 1. Theory and range of validity. *J. Am. Chem. Soc. 104*, 4546−4559.
(41) Lipari, G., and Szabo, A. (1982) Model-free approach to the interpretation of nuclear magnetic resonance relaxation in macromolecules. 2. Analysis of experimental results. *J. Am. Chem. Soc. 104*, 4559−4570.
(42) Clore, G. M., Driscoll, P. C., Wingfield, P. T., and Gronenborn, A. M. (1990) Analysis of backbone dynamics of interleukin-1β using two-dimensional inverse detected heteronuclear ^{15}N-^{1}H NMR spectroscopy. *Biochemistry 29*, 7387−7401.
(43) Clore, G. M., Szabo, A., Bax, A., Kay, L. E., Driscoll, P. C., and Gronenborn, A. M. (1990) Deviations from the simple two parameter model free approach to the interpretation of ^{15}N nuclear magnetic relaxation of proteins. *J. Am. Chem. Soc. 112*, 4989−4991.
(44) Cole, R., and Loria, J. P. (2003) FAST-Modelfree: A program for rapid automated analysis of solution NMR spin-relaxation data. *J. Biomol. NMR 26*, 203−213.
(45) Mandel, A. M., Akke, M., and Palmer, A. G. (1995) Backbone dynamics of *Escherichia coli* ribonuclease HI: Correlations with structure and function in an active enzyme. *J. Mol. Biol. 246*, 144−163.
(46) Palmer, A. G., Rance, M., and Wright, P. E. (1991) Intramolecular motions of a zinc finger DNA-binding domain from Xfin characterized by proton-detected natural abundance ^{13}C heteronuclear NMR spectroscopy. *J. Am. Chem. Soc. 113*, 4371−4380.
(47) Bieri, M., and Gooley, P. R. (2011) Automated NMR relaxation dispersion data analysis using NESSY, BMC. *Bioinformatics 12*, 421.
(48) Akaike, H. (1980) Likelihood and the Bayes procedure. In *Bayesian Statistics* (Bernardo, J. M., et al., Eds.) University Press, Valencia, Spain.
(49) Tugarinov, V., and Kay, L. E. (2003) Quantitative NMR studies of high molecular weight proteins: Application to domain orientation and ligand binding in the 723 residue enzyme malate synthase G. *J. Mol. Biol. 327*, 1121−1133.
(50) Hodsdon, M. E., and Cistola, D. P. (1997) Discrete backbone disorder in the nuclear magnetic resonance structure of apo intestinal fatty acid-binding protein: Implications for the mechanism of ligand entry. *Biochemistry 36*, 1450−1460.
(51) Englander, S. W., and Kallenbach, N. R. (1983) Hydrogen exchange and structural dynamics of proteins and nucleic acids. *Q. Rev. Biophys. 16*, 521−655.
(52) Gryk, M. R., and Jardetzky, O. (1996) AV77 hinge mutation stabilizes the helix-turn-helix domain of trp repressor. *J. Mol. Biol. 255*, 204−214.
(53) Gryk, M. R., Finucaine, M. D., Zheng, Z., and Jardetzky, O. (1995) Solution dynamics of the trp repressor: A study of amide proton exchange by T1 relaxation. *J. Mol. Biol. 246*, 618−627.
(54) Phan, I. Q. H., Boyd, J., and Campbell, I. D. (1996) Dynamic studies of a fibronectin type I module pair at three frequencies: Anisotropic modelling and direct determination of conformational exchange. *J. Biomol. NMR 8*, 369−378.
(55) Palmer, A. G., Kroenke, C. D., and Loria, J. P. (2001) Nuclear magnetic resonane methods for quantifying microsecond-to-millisecond motions in biological macromolecules. *Methods Enzymol. 339*, 204−238.
(56) Pritchard, D. M., and Watson, A. J. (1996) Apoptosis and gastrointestinal pharmacology. *Pharmacol. Ther. 72*, 149−169.
(57) Palmer, A. G. (1993) Dynamic properties of proteins from NMR spectroscopy. *Curr. Opin. Biotechnol. 4*, 385−391.
(58) Eletsky, A., Kienhofer, A., Hilvert, D., and Pervushin, K. (2005) Investigation of ligand binding and protein dynamics in *Bacillus subtilis* chorismate mutase by transverse relaxation optimized spectroscopy-nuclear magnetic resonance. *Biochemistry 44*, 6788−6799.
(59) Freedberg, D. I., Ishima, R., Jacob, J., Wang, Y. X., Kustanovich, I., Louis, J. M., and Torchia, D. A. (2002) Rapid structural fluctuations of the free HIV protease flaps in solution: Relationship to crystal structures and comparison with predictions of dynamics calculations. *Protein Sci. 11*, 221−232.
(60) Butterwick, J. A., Loria, J. P., Astrof, N. S., Kroenke, C. D., Cole, R., Rance, M., and Palmer, A. G. (2004) Multiple time scale backbone dynamics of homologous thermophilic and mesophilic ribonuclease HI enzymes. *J. Mol. Biol. 339*, 855−871.
(61) Kovrigin, E. L., Cole, R., and Loria, J. P. (2003) Temperature dependence of the backbone dynamics of ribonuclease A in the ground state and bound to the inhibitor 5′-phosphothymidine (3′-5′)-pyrophosphate adenosine 3′-phosphate. *Biochemistry 42*, 5279−5291.

(62) Eliseo, T., Ragona, L., Catalano, M., Assfalg, M., Paci, M., Zetta, L., Molinari, H., and Cicero, D. O. (2007) Structural and dynamic determinants of ligand binding in the ternary complex of chicken liver bile acid binding protein with two bile salts revealed by NMR. *Biochemistry 46*, 12557−12567.
(63) Cogliati, C., Tomaselli, S., Assfalg, M., Pedò, M., Ferranti, P., Zetta, L., Molinari, H., and Ragona, L. (2009) Disulfide bridge regulates ligand-binding site selectivity in liver bile acid-binding proteins. *FEBS J. 276*, 6011−6023.
(64) Cogliati, C., Ragona, L., D'Onofrio, M., Günther, U., Whittaker, S., Ludwig, C., Tomaselli, S., Assfalg, M., and Molinari, H. (2010) Site-specific investigation of the steady-state kinetics and dynamics of the multistep binding of bile acid molecules to a lipid carrier protein. *Chem.—Eur. J. 16*, 11300−11310.
(65) Corsico, B., Cistola, D. P., Frieden, C., and Storch, J. (1998) The helical domain of intestinal fatty acid binding protein is critical for collisional transfer of fatty acids to phospholipid membranes. *Proc. Natl. Acad. Sci. U.S.A. 95*, 12174−12178.
(66) Liou, H. L., Kahn, P. C., and Storch, J. (2002) Role of the helical domain in fatty acid transfer from adipocyte and heart fatty acid-binding proteins to membranes: Analysis of chimeric proteins. *J. Biol. Chem. 277*, 1806−1815.
(67) Lücke, C., Zhang, F., Rüterjans, H., Hamilton, J. A., and Sacchettini, J. C. (1996) Flexibility is a likely determinant of binding specificity in the case of ileal lipid binding protein. *Structure 4*, 785−800.
(68) Lücke, C., Fushman, D., Ludwig, C., Hamilton, J. A., Sacchettini, J. C., and Rüterjans, H. (1999) A comparative study of the backbone dynamics of two closely related lipid binding proteins: Bovine heart fatty acid binding protein and porcine ileal lipid binding protein. *Mol. Cell. Biochem. 192*, 109−121.
(69) Pedo, M., Löhr, F., D'Onofrio, M., Assfalg, M., Dötsch, V., and Molinari, H. (2009) NMR studies reveal the role of biomembranes in modulating ligand binding and release by intracellular bile acid binding proteins. *J. Mol. Biol. 384*, 852−863.